Projected climate change in Finland during the 21st century calculated from CMIP6 model simulations

Kimmo Ruosteenoja and Kirsti Jylhä

Finnish Meteorological Institute, P.O. Box 503, FI-00101 Helsinki, Finland
Corresponding author, `kimmo.ruosteenoja@fmi.fi`

Abstract

Climate scenarios for Finland were updated to correspond the Shared Socioeconomic Pathway (SSP) greenhouse gas (GHG) scenarios, considering nearly 30 global climate models (GCMs) that participated in Phase 6 of the Coupled Model Intercomparison Project (CMIP6). The SSPs and CMIP6 GCMs had also been used by the Intergovernmental Panel on Climate Change (IPCC) in composing the Sixth Assessment Report, published in 2021. Projections are provided for three future 30-year periods and all four SSP scenarios from which enough GCM data were available.

The signs and geographical patterns of the projected changes are mostly similar to those derived from the previous model generation, the amplitude of the changes depending on the GHG scenario. For example, by the period 2040–2069 under SSP2-4.5, mean temperatures are projected to increase in Finland by 2.4 (1.0–3.8) °C in summer and 3.3 (1.2–5.4) °C in winter (the multi-model mean change relative to 1981– 2010 and, in parentheses, the 90 % uncertainty interval reflecting inter-model differences). Compared to the projections calculated from the previous model generations using comparable GHG scenarios (RCP4.5 or SRES B1), warming is fairly similar in winter but stronger in summer. The diurnal range of temperature is projected to be reduced in the cold season.

Precipitation increases by 5 (−6 to 17) % in summer and 12 (0 to 24) % in winter, in good concordance with the previous projections. In summer, the sign of change is fairly uncertain, particularly in southern Finland. Estimates for seasonal incident solar radiation change have become brighter by 1– 4 percentage points. For air pressure and wind speed, the multi-model mean changes are close to zero but inter-model spread is sizeable.

Keywords: Climate change; CMIP6 models; SSP scenarios; surface air temperature; precipitation; solar radiation; diurnal temperature range

1 Introduction

The previous comprehensive update of model-derived climate projections for Finland was published more than five years ago (*Ruosteenoja et al.*, 2016a, hereafter referred to RJK16). Thereafter, a new generation of global climate models (GCMs) participating in Phase 6 of the Coupled Model Intercomparison Project (CMIP6, *Eyring et al.*, 2016) has become available. Moreover, new greenhouse gas scenarios are now used, termed the Shared Socioeconomic Pathways (SSPs, *O'Neill et al.*, 2016; *Riahi et al.*, 2017). The SSP scenarios and CMIP6 GCM simulations constitute the data basis for the climate projections presented in the Sixth Assessment Report of the Intergovernmental Panel on Climate

Change (*IPCC*, 2021). Accordingly, it is topical to update the Finnish climate scenarios to correspond to the current greenhouse gas scenarios and GCMs.

For composing climate change estimates for the future, GCMs constitute the primary tool. GCMs are simulation models that build on the laws of physics governing the climate system of the Earth; the main components of the system are the atmosphere, oceans, cryosphere and near-surface soil layer. Owing to limitations in the available computing capacity, in GCMs many physical processes have to be represented in a simplified manner. These simplifications have been implemented in a different way in the various models, and therefore simulated future climatic changes diverge across the GCMs. In order to obtain a reliable picture of future changes and, in particular, the related uncertainties, it is therefore of utmost importance to analyse a large ensemble of GCMs (e.g., *Stolpe et al.*, 2021)

Since the 1990s, scenarios for future climate in Finland have been produced in numerous studies (e.g., *Carter et al.*, 1996; *Fortelius et al.*, 1996; *Jylhä et al.*, 2004, 2009; *Ruosteenoja et al.*, 2013; *Lehtonen et al.*, 2016a) and RJK16. Climate change scenarios derived from previous model generations are likewise available for our neighbouring countries, e.g., for Estonia (*Jaagus and Mändla*, 2014; *Sepp et al.*, 2018), Latvia (*Ruosteenoja et al.*, 2016b), Norway (*Hanssen-Bauer et al.*, 2017) and Sweden (*Eklund et al.*, 2015; *Kjellström et al.*, 2016).

Climate scenarios have been utilized to explore various impacts of climate change in Finland, including adaptation research. RJK16 listed a multitude of such studies; here, examples of more recent work are given. *Olsson et al.* (2015) showed that spring floods in rivers will start earlier and be weaker in the future while winter discharges increase. Shorter and milder winters weaken the ground-bearing capacity in forests and forest truck roads, thus deteriorating the preconditions of harvesting and transportation of timber (*Lehtonen et al.*, 2019). A comprehensive summary dealing with the impacts of climate change on the Finnish forests and forestry was presented in *Venäläinen et al.* (2020). The impact of warming autumns on crop production in Finland was explored by *Peltonen-Sainio et al.* (2018). *Jylhä et al.* (2020) produced weather data for studies of building physics and energy consumption in the changing climate, and, utilizing this dataset, the risk of hot weather and related overheating of apartments was explored by *Velashjerdi Farahani et al.* (2021). Due to increases in the amount of wind-driven rain and less favourable drying conditions in the future, the corrosion rate of structures exposed to outdoor conditions will increase in Finland, most notably in winter (*Pakkala et al.*, 2019). In the study by *Saranko et al.* (2020), climate scenarios for the city of Vantaa were further downscaled using an air-surface interaction model with a horizontal resolution of 500 m.

According to *Mikkonen et al.* (2015), annual mean temperature in Finland might have increased by more than 2 °C since the mid-19th century to the 2010s, but this estimate is subject to large uncertainty due to the sparse network of observation sites in the early decades of the period (*Tietäväinen et al.*, 2010). Studying a period from the beginning of the 20th century to the present, *Ruosteenoja and Räisänen* (2021) reported a warming of slightly smaller than 2 °C. Furthermore, it turned out that GCMs as a collective were able to reproduce this long-term warming rather closely. This finding supports the idea that

GCMs can successfully be utilized in building future projections as well.

In concordance with the increasing temperatures in the cold season, snow depth in Finland has decreased after 1961 and the number of days with snow cover has abated (*Aalto et al.*, 2016; *Luomaranta et al.*, 2019). According to *Aalto et al.* (2016), during this period the mean daily minimum temperatures have increased somewhat more rapidly than the maxima. Conversely, no statistically significant trends were detected in the country-wide averages of precipitation and surface air pressure. According to *Jylhä et al.* (2014), in southern Finland incident solar radiation has increased in autumn by 5 % per decade during 1980–2009; in the other seasons and annually, the changes were not statistically significant but subject to decreases in diffuse and increases in direct solar radiation. Considering an average of 33 Finnish observation sites, *Laapas and Venäläinen* (2017) reported a minor negative trend ($-0.09\,\mathrm{m\,s^{-1}}$ per decade) in the annual-mean wind speed in 1959–2015.

In this paper, our focus is on the moderate-emission SSP2-4.5 scenario rather than the high-emission Representative Concentration Pathway RCP8.5 emphasized in RJK16. This scenario has been selected because in the recent years there have been substantial advances in global climate policy, and consequently a sustained increase in greenhouse gas emissions throughout this century, as assumed in RCP8.5, appears quite unlikely. Climate change projections are produced for the mean temperature, precipitation, surface pressure, incident solar radiation, diurnal temperature range and wind speed. In addition, some tentative results are shown for relative humidity. Unlike in RJK16, the present projections are exclusively derived from global models, since representative ensembles of regional climate model (RCM) simulations to downscale the CMIP6 GCM output have not yet been published (*Giorgi et al.*, 2021).

The outline of the present paper is the following. First, in section 2, we introduce the greenhouse gas scenarios, GCMs included in the analysis and the techniques used in creating the climate scenarios. Section 3 deals with future changes in the Finnish climate on the annual, seasonal and monthly mean level. Moreover, the spatial distributions of changes in four key climate variables are shown for the European area. Section 4 compares the present projections with those derived from the previous model generations. The paper is closed by the summary and conclusions section (section 5).

2   Data and methods

2.1   SSP scenarios

In this work, we elaborate climate projections for those four SSP greenhouse gas scenarios for which data are available from a sufficient number of GCMs for scenario production. The SSP scenarios are described in detail in *O'Neill et al.* (2016) and *Riahi et al.* (2017). The number at the end of the acronym of the scenario reveals the approximate magnitude of radiative forcing around 2100; for instance, if the SSP2-4.5 scenario were realized, radiative forcing at the end of this century would be about $4.5\,\mathrm{W\,m^{-2}}$ (*IPCC*, 2021). Accordingly, of the four scenarios examined, SSP1-2.6 represents the lowest, SSP2-4.5 medium-level, SSP3-7.0 rather high and SSP5-8.5 very high radiative forcing. Note that

SSP1-2.6, SSP2-4.5 and SSP5-8.5 are updates of the old RCP2.6, RCP4.5 and RCP8.5 scenarios while SSP3-7.0 fills the gap between RCP6.0 and RCP8.5 (*O'Neill et al.*, 2016). Besides these four SSP scenarios, *IPCC* (2021) examines a greenhouse-gas scenario with very low emissions (SSP1-1.9), representing a pathway towards the very stringent 1.5 °C global warming target. In the present study, this scenario had to be excluded due to a small number of GCM simulations available.

Each SSP scenario provides information about the future emissions of carbon dioxide, methane, nitrous oxide and other greenhouse gases, as well as the precursors of aerosol particles. The by far most important anthropogenic greenhouse gas is carbon dioxide (CO_2) that, according to all four SSP scenarios considered here, accounts for about 80 % of human-induced radiative forcing in 2100 (*Meinshausen et al.*, 2020). The temporal evolution of the CO_2 emissions under the four SSPs is shown in Fig. 1. Even though the nominal radiative forcing in the equivalent RCP and SSP scenarios is the same, the emissions of individual greenhouse gases are not identical. For example, the emissions of carbon dioxide are far larger in SSP5-8.5 than in RCP8.5, but this is partially compensated by lower emissions of methane and nitrous oxide (*Meinshausen et al.*, 2020).
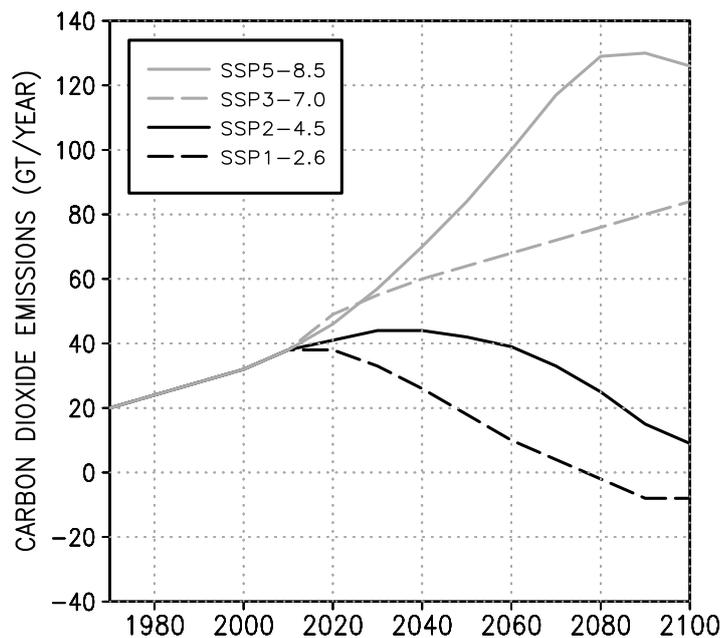

Fig. 1: Global emissions of carbon dioxide in gigatonnes per year in 1970–2100 according to four SSP scenarios; see the legend. Re-drawn using the data given in Fig. 3a of *O'Neill et al.*, 2016.

According to the recently-published Sixth Assessment Report of *IPCC* (2021, Table SPM.1), SSP1-2.6, SSP2-4.5, SSP3-7.0 and SSP5-8.5 would produce a global-mean temperature increase of 1.8 (uncertainty interval 1.3–2.4), 2.7 (2.1–3.5), 3.6 (2.8–4.6) and 4.4 (3.3–5.7) degrees, respectively, by the period 2081–2100 relative to the preindustrial

level. According to Fig. 1, under SSP3-7.0 CO_2 emissions would double and under SSP5-8.5 become three-fold compared to the level that prevailed in the 2010s. Both of these two high-emission scenarios are thus strongly inconsistent with the official targets of the global climate policy, i.e., to curtail greenhouse gas emissions and to limit the resulting global warming below 2 °C or even 1.5 °C relative to the preindustrial era (*IPCC*, 2021). On the other hand, to attain the low-emission SSP1-2.6 pathway, far more ambitious reductions in the emissions would be needed than what the countries have engaged themselves hitherto. In the second half of the century, even negative net emissions would be needed; this indicates that anthropogenic removal of CO_2 must exceed the global emissions. Consequently, in the present study the main focus is on SSP2-4.5. According to that scenario, the emissions of CO_2 start to decline around 2040, and at the end of this century, they have dropped to about one fourth of the current level (Fig. 1). As a consequence, the atmospheric concentration of CO_2 would stabilize and be approximately double that prior to the industrialization (*O'Neill et al.*, 2016, Fig. 3).

2.2   GCM data

The CMIP6 GCMs that were utilized in building the climate projections are listed in Table 1. Additional information about the models is given in Annex II of *IPCC* (2021). GCM output data were downloaded from the data archives of the Earth System Grid Federation. For more information about the output data files and data preprocessing, consult section 2 of *Ruosteenoja* (2021, hereafter referred to R21).

In R21, 37 CMIP6 GCMs were evaluated by studying their ability to adequately simulate the global-mean temperature, both regarding past trends and the consistency of future responses to the four SSP forcing scenarios. Also, the performance of the GCMs in simulating recent past climate in southern and northern Europe and globally was considered. Furthermore, it was required that a GCM has to provide data for four key climate variables, namely the near-surface air temperature, precipitation, sea-level pressure and incident solar radiation, and the values of these four variables have to be physically reasonable at all grid points throughout the simulation period. Moreover, no more than two model versions from any individual research centre were incorporated in the analysis. GCMs having obtained low ratings in this evaluation were rejected. Those 28 GCMs that showed, at the very least, tolerable performance, i.e., having deserved two or three stars in Table 2 of R21, were included in the calculations.

Accordingly, for temperature, precipitation, pressure and solar radiation, data were available from all 28 GCMs (Table 1). For the remaining variables explored (relative humidity, daily minimum and maximum temperature and wind speed) data were missing from some models. As evidenced in R21, the daily temperature extremes were additionally erroneous or unrealistic in three GCMs: CMCC-CM2-SR5, NESM3, and AWI-CM-1-1-MR. Furthermore, in *Ruosteenoja et al.* (2019) wind speed changes produced by the previous-generation models originating from GFDL were shown to be spuriously influenced by changes in the ground properties. Within the CMIP6 ensemble, GFDL-ESM4 similarly yielded a wind speed response strongly deviating from all other GCMs. This

Table 1: Availability of the various climate variables and the number of parallel runs for the different GCMs. Explanations: ∗: data for the variable are available; –: data are missing completely; (–): data are missing from so many model runs that it could not be used; D: data had to be rejected owing to technical issues or low quality. Variables: `temp` stands for the mean temperature, `prec` for precipitation, `slp` sea level pressure, `rad` incident solar radiation, `rh` relative humidity, t_{nx} the minimum and maximum temperature of the day, and `wind` near-surface wind speed. The five columns on the right show the count of parallel runs analyzed for the historical period (`hist`) and the four SSP scenarios (numbers; e.g., '126' refers to the SSP1-2.6 scenario). For some GCMs, the number of parallel runs varies depending on the variable.

	Model	Country	temp	prec	slp	rad	rh	t_{nx}	wind	hist	126	245	370	585
1	MIROC6	Japan	∗	∗	∗	∗	∗	∗	∗	10	10	3	3	10
2	MRI-ESM2-0	Japan	∗	∗	∗	∗	∗	∗	∗	5	1	1	5	1
3	TaiESM1	China (Taipei)	∗	∗	∗	∗	–	–	∗	1	1	1	1	1
4	BCC-CSM2-MR	China (Peoples)	∗	∗	∗	∗	(–)	∗	∗	3	1	1	1	1
5	CAMS-CSM1-0	China (Peoples)	∗	∗	∗	∗	–	–	∗	2	2	2	2	2
6	NESM3	China (Peoples)	∗	∗	∗	∗	–	D	(–)	5	2	2	–	2
7	INM-CM4-8	Russia	∗	∗	∗	∗	∗	∗	∗	1	1	1	1	1
8	INM-CM5-0	Russia	∗	∗	∗	∗	∗	∗	∗	10	1	1	5	1
9	NorESM2-LM	Norway	∗	∗	∗	∗	∗	–	∗	3	1	3	1	1
10	NorESM2-MM	Norway	∗	∗	∗	∗	∗	–	∗	3	1	2	1	1
11	HadGEM3-GC31-LL	Britain	∗	∗	∗	∗	∗	∗	∗	4	1	1	–	4
12	UKESM1-0-LL	Britain	∗	∗	∗	∗	∗	∗	∗	7	10	5	10	5
13	MPI-ESM1-2-HR	Germany	∗	∗	∗	∗	∗	∗	∗	10	2	2	10	2
14	MPI-ESM1-2-LR	Germany	∗	∗	∗	∗	∗	∗	∗	10	10	10	10	10
15	AWI-CM-1-1-MR	Germany	∗	∗	∗	∗	(–)	D	∗	3	1	1	3	1
16	CNRM-CM6-1	France	∗	∗	∗	∗	∗	∗	∗	10	6	6	6	6
17	CNRM-ESM2-1	France	∗	∗	∗	∗	∗	∗	∗	9	5	8	5	5
18	IPSL-CM6A-LR	France	∗	∗	∗	∗	∗	∗	∗	10	5	7	10	5
19	CMCC-CM2-SR5	Italy	∗	∗	∗	∗	∗	D	∗	1	1	1	1	1
20	EC-Earth3	European Union	∗	∗	∗	∗	∗	∗	∗	6	4	6	4	4
21	EC-Earth3-Veg	European Union	∗	∗	∗	∗	∗	∗	∗	4	3	4	2	2
22	CESM2	United States	∗	∗	∗	∗	∗	(–)	∗	10	5	4	7	5
23	CESM2-WACCM	United States	∗	∗	∗	∗	∗	(–)	∗	3	1	5	1	5
24	GFDL-ESM4	United States	∗	∗	∗	∗	∗	∗	D	3	1	3	1	1
25	GISS-E2-1-G	United States	∗	∗	∗	∗	∗	∗	∗	10	1	10	10	1
26	CanESM5	Canada	∗	∗	∗	∗	∗	∗	∗	10	10	10	10	10
27	ACCESS-CM2	Australia	∗	∗	∗	∗	∗	∗	∗	3	3	3	3	3
28	ACCESS-ESM1-5	Australia	∗	∗	∗	∗	∗	∗	∗	10	10	10	10	10

GCM had thereby to be excluded from wind speed calculations. Accordingly, the projections of the wind speed, relative humidity and diurnal temperature range are derived from 26, 23, and 19 GCMs, respectively (Table 1). This implies that projections for the different variables are calculated from somewhat dissimilar model ensembles and are thus not wholly commensurate. Note also that the relative humidity data files were not checked as profoundly as was done for the other variables, and consequently the present humidity projections should be regarded as tentative.

R21 calculated future annual-mean projections for Finland for three variables by varying the size of the GCM ensemble from 24 to 37. Fig. 16 of that report indicates that the mean temperature and precipitation projections are very similar regardless of the ensemble size, whereas solar radiation is somewhat more sensitive.

All the GCM data used in this work were given as the time series of monthly means. Historical runs, covering the years 1850–2014, are forced by observational greenhouse gas concentrations. Scenario runs representing the four SSPs extend from 2015 to 2099 or 2100.

For many GCMs, several parallel runs have been carried out. In the parallel runs, the evolution of the greenhouse gas concentrations and other forcing agents is identical but the initial conditions diverge. The purpose of parallel runs is to unfold the contribution of internal variability in the climate system. By inspecting multiple parallel runs it is possible to improve the statistical robustness of the projection. In the present analysis, we have included all the parallel runs available for each GCM and scenario; however, to avoid excessive use of computing resources and storing capacity, the maximum count of runs for an individual GCM has been limited to 10 (Table 1). This reduces the uncertainty stemming from inter-realization differences by a factor of $1/\sqrt{10}$ or ~ 0.3.

2.3   Building the climate change projections

Model data were given on the original grids of the GCMs. To calculate the multi-model means and standard deviations, the data were interpolated onto a common global 2.5×2.5 degree grid by using the first order conservative remapping (*Jones*, 1999); for more information, see section 2.1 of R21.

Long-term climate changes were uncovered by calculating 30-year running means from the model output, separately for the individual months, four seasons and annual means. Then, for each model and SSP scenario, the responses of the individual parallel runs were averaged, only including those parallel runs for which data were available for both the historical and scenario period. Finally, multimodel means were calculated by giving an equal weight for all GCMs. As discussed in *Weigel et al.* (2010), a non-equal weighting would be difficult to justify since there is no definite quantitative information on the performance of the individual models in simulating future climate. Spatial averages of Finland were obtained as the area-weighted means of 11 grid squares. Henceforth, unless otherwise stated, all the climate projections presented for Finland are derived from these spatial averages.

All the climate responses were calculated relative to the baseline-period 1981–2010.

Three scenario periods are considered: 2020–2049, 2040–2069, and 2070–2099. In the most recent normal period, 1991–2020, the national annual mean temperature of Finland was approximately 0.6 °C higher than in 1981–2010 (*Jokinen et al.*, 2021).

For the SSP1-2.6, SSP2-4.5, and SSP5-8.5 scenarios, simulations are available for all the GCMs, while for SSP3-7.0, data are missing from NESM3 and HadGEM3-GC31-LL (Table 1). For these two GCMs, surrogate data for SSP3-7.0 were created by using the scaling procedure described in detail in Appendix A1 of RJK16. Note that in the present GCM ensemble, the proportion of missing runs is substantially smaller than in RJK16, and consequently the use of scaling has very little impact on the multi-model responses. The projected changes of incident solar radiation are strongly affected by aerosol forcing and are thus not proportional to the global-mean temperature change (R21, Fig. 16). Since this would constitute a prerequisite for the use of scaling, no scaling was conducted to solar radiation. Therefore, for this variable the responses to SSP3-7.0 were derived from those 26 GCMs that genuinely provide data.

The multi-model mean change is used to represent the best estimate for the future response. To derive 90 % uncertainty intervals for the change (from the 5th to the 95th percentile), we fitted a normal distribution to the ensemble of the responses produced by the GCMs, yielding

$$\bar{x} \pm 1.645\sigma \;,$$

where $\bar{x}$ stands for the mean and σ for the standard deviation of the modelled changes.

Following the approach of *Stolpe et al.* (2021), the inter-model standard deviation σ was calculated from the responses produced by the first parallel run of each GCM. The resulting estimate is unbiased and takes into consideration both the true inter-model differences and the contribution of internal variability. On the other hand, data from the higher parallel runs is now omitted, which acts to decline the robustness of the estimated σ. The present procedure deviates from the more sophisticated algorithm employed in RJK16 that utilised information from all the parallel runs available in calculating the standard deviation (RJK16, Appendix A2). Nevertheless, the old method had to be rejected since it assumed that the scatter across the parallel runs needs to be identical in all GCMs. Figs. 1, 6, 7, and 8 of R21 indicate that this assumption does not hold in reality.

The reader has to be aware that our approach to derive the mean temperature projections differs from that used in *IPCC* (2021). In the first time of the history of IPCC, in the fresh assessment report temperature projections are not determined purely by the GCM simulations of future climate but observational constraints and the assessed climate sensitivity have been taken into account as well. For the other atmospheric variables discussed in the present paper, by contrast, projections have been derived directly from GCM simulations, both in *IPCC* (2021) and the present work.

3   Future changes

3.1   Annual mean responses

The evolution of the annual multi-model mean temperature and precipitation is depicted in Fig. 2. Annual and seasonal changes for all six variables for three future periods are shown in Tables S1–S6 of the Supplement.
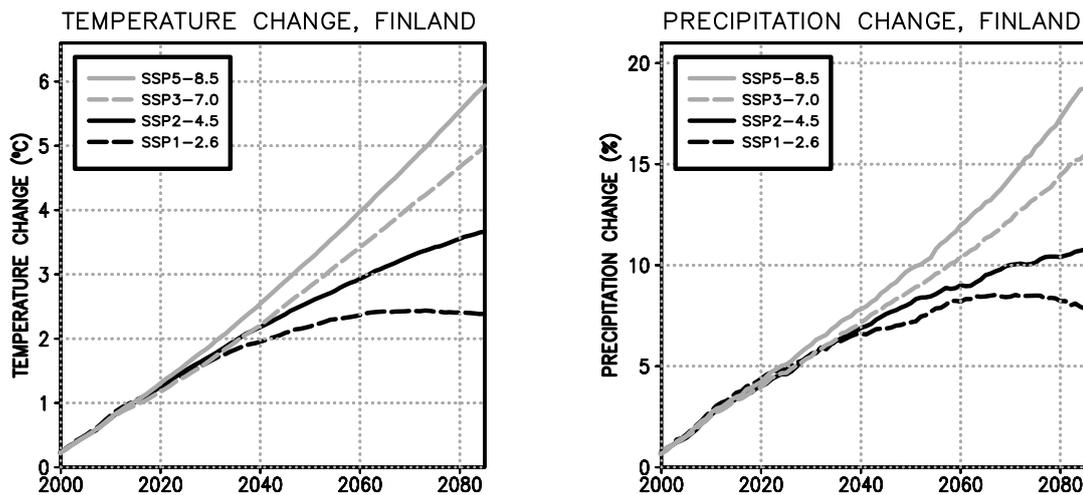

Fig. 2: Multi-model mean changes in annual mean surface air temperature (in °C; left panel) and precipitation (in %; right panel) for the years 2000–2085, relative to the mean of the baseline period 1981–2010. The curves show 30-year running means of the spatial averages of Finland. Projections are given for four greenhouse gas scenarios: SSP5-8.5, SSP3-7.0, SSP2-4.5 and SSP1-2.6 (see the legend).

During the next few decades, warming continues under all four forcing scenarios, but the responses represented as 30-year running means start to diverge increasingly after the 2040s. In the two high-emission scenarios, warming continues at a constant pace by the late 21st century and evidently even beyond. According to SSP5-8.5, the mean temperature of Finland would increase by nearly 6 °C in nine decades; under SSP3-7.0, the corresponding warming amounts to 5 °C. Curtailing the greenhouse-gas emissions reduces the strength of warming substantially; under SSP2-4.5 (SSP1-2.6) by the 2080s, warming would be 3.7 °C (2.4 °C), i.e., about 60 % (40 %) of that under the most severe SSP5-8.5 scenario. Compared to the temperatures simulated for the early 2020s, SSP2-4.5 would entail additional warming of 2.5 °C, SSP1-2.6 only slightly more than 1 °C. Under SSP1-2.6, warming would cease after the mid-century. Admittedly, all these figures are subject to sizeable inter-model differences in the simulated warming. This topic will be discussed in subsection 3.2.

Concurrently, the annual precipitation sum is projected to increase by 8–19 %, depending on the SSP scenario (Fig. 2). As will be discussed below, this increase is likely to be distributed quite unevenly over the seasons.

Compared to the global mean warming, the projected increase of mean temperature in Finland appears to be substantially more rapid (Fig. 3). In the early decades of this century, the ratio of the Finnish to global warming relative to 1981–2010 is close to 2 or even higher, but when examining longer timescales, the ratio converges towards ~ 1.6. The rapid warming of Finland during the first few decades of the period may be related to various feedback processes in the climate system. For example, in the early 21$^{\text{st}}$ century ice edge in the Arctic Ocean is situated relatively close to our country, the ongoing ice retreat thus affecting the Finnish temperatures substantially. Later in this century, ice-free water areas in the European sector of the Arctic Ocean will be far wider. An additional factor amplifying warming in Finland in the early-21$^{\text{st}}$ century may be the weakening aerosol dimming in Europe. Fig. 4 indicates that, within the GCM ensemble, there is a distinct positive linkage between the modelled future warming in Finland and in the global scale (correlation coefficient ~ 0.8); those GCMs that produce a strong global-mean temperature increase also tend to simulate large warming for Finland, even though the dependence is by no means perfect.
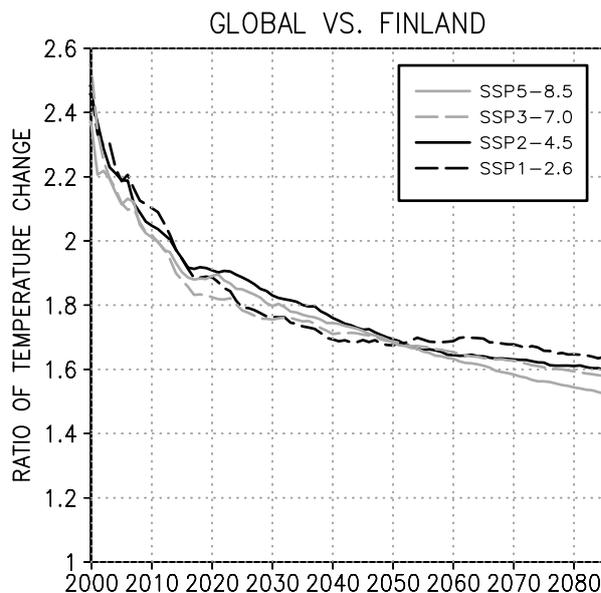
Fig. 3: Ratio of multi-model annual mean temperature change in Finland (relative to 1981–2010) to the corresponding global mean temperature change for the years 2000–2085. The ratios are given for four greenhouse gas scenarios: SSP5-8.5, SSP3-7.0, SSP2-4.5, and SSP1-2.6 (see the legend).

Note that Fig. 3 depicts the ratios for the absolute changes of the annual mean temperature between two discrete time periods, e.g., '2060' indicating a change from 1981–2010 to 2045–2074. The ratios of the actual warming speeds (time derivatives) were also studied, but they proved to be very noisy in time and are therefore not shown here. During the second half of the 21$^{\text{st}}$ century, the ratio of the Finnish to global warming speed is ~ 1.4.
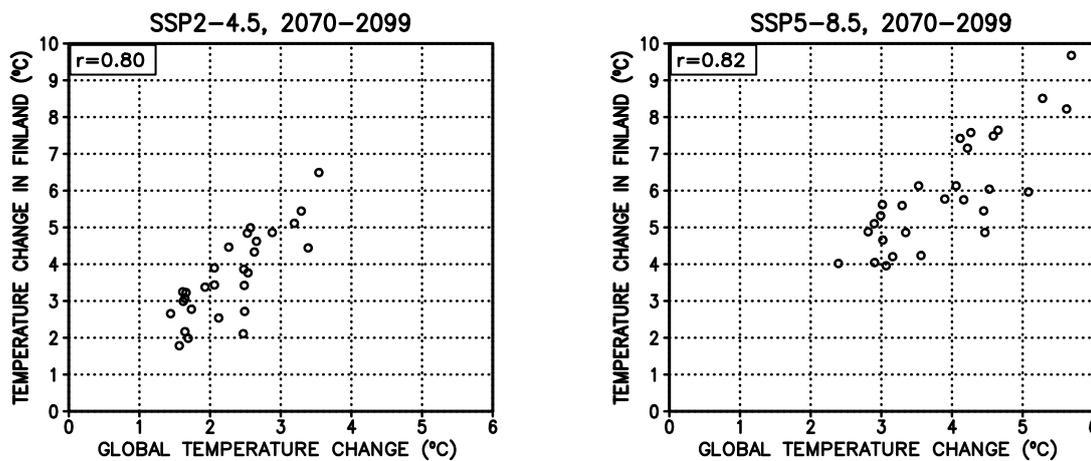
Fig. 4: Annual-mean temperature change in Finland as a function of the global-mean change for the period 2070–2099, relative to 1981–2010; responses produced by the 28 GCMs under the SSP2-4.5 (left) and SSP5-8.5 (right) scenarios. The correlation coefficients between the changes are given on the top-left corners of the panels.

One interesting question is whether the GCM ensemble manifests any dependence between the simulated baseline-period climate and the rate of future warming. Fig. 5 and Fig. S1 in the Supplement indicate that no relationship exists, at least, in Finland; the modelled warming appears to be independent of the mean temperatures simulated for the period 1981–2010. This finding is in line with *Jylhä et al.* (2004) who reported the absence of such a relationship in an ensemble of six contemporary GCMs.

3.2   Seasonal changes

Projected changes in six basic climate variables under SSP2-4.5 for two future periods are shown in Figs. 6 and S2. Both the best-estimate (multi-model mean) changes and the 5 to 95 % uncertainty intervals are depicted. Corresponding information at the seasonal and annual mean level is presented in Tables S1–S6 in the Supplement file, considering all three projection periods and four SSPs.

Temperatures will increase in all seasons, most likely more strongly in winter than in summer. The GCMs are very concordant on the sign of change, but there is substantial divergence in the magnitude. For example, considering the mid-century climate, in mid-winter the 90 % probability interval of the temperature increase is from 1 °C to 6 °C, in summer from 1 °C to 4 °C. The diurnal temperature range is likely to remain nearly unchanged in summer, the daily minima and maxima increasing nearly at an equal pace. From November to April, the range is projected to be reduced. Note that in early and mid-winter in particular, the diurnal temperature range is mainly determined by synoptic weather variations within the day rather than by the regular cycle between mild day-time and cold night-time temperatures.
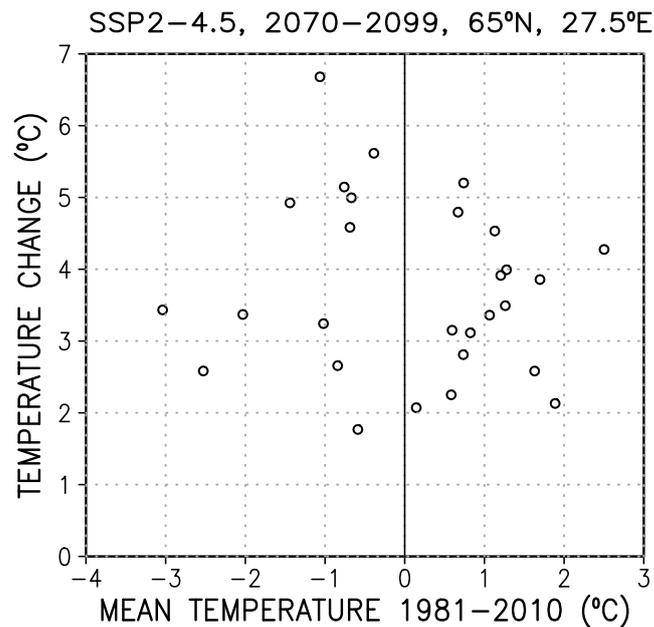
Fig. 5: Annual mean temperature change (1981–2010 → 2070–2099) under SSP2-4.5 as a function of the baseline-period (1981–2010) mean temperature at 65°N, 27.5°E in the 28 GCMs. Unit: °C.

For the other four variables, the models more or less disagree on the sign of change. In particular, for the wind-speed and surface air pressure reduced to the sea level, the best-estimate changes are close to zero, even though a minor calming of winds may take place in mid to late summer. Considering the inter-model scatter, changes in monthly mean wind speeds potentially amount to −12 to +10 % by the 2080s (Fig. S2). Precipitation is more likely to increase than decrease in all seasons, but in summer the direction of the change is very uncertain. Solar radiation may to some extent increase in summer and early autumn and decrease in late autumn and winter. Accordingly, the contrast between the abundantly light-rich summers and dark winters is projected to deepen further.

Furthermore, we compared the multi-GCM mean changes in temperature and precipitation between northern and southern Finland, the boundary between the regions being 64°N (Fig. 7). The temperature projections are nearly identical for both regions apart from November-December, when warming is slightly stronger in the north than south. For precipitation, by contrast, the largest differences occur in the warm season. From July to September, precipitation is projected to increase by 4–8 % in northern Finland while remaining nearly unchanged in the south. Owing to intensifying evapotranspiration induced by the increasing temperatures, the risk for summer drought thereby increases in the south.

As stated above, for the relative humidity the present projections are only provisional. There are two reasons for this. Firstly, the quality of the humidity simulations in the individual GCMs was not explored in the model evaluation report (R21). Sec-
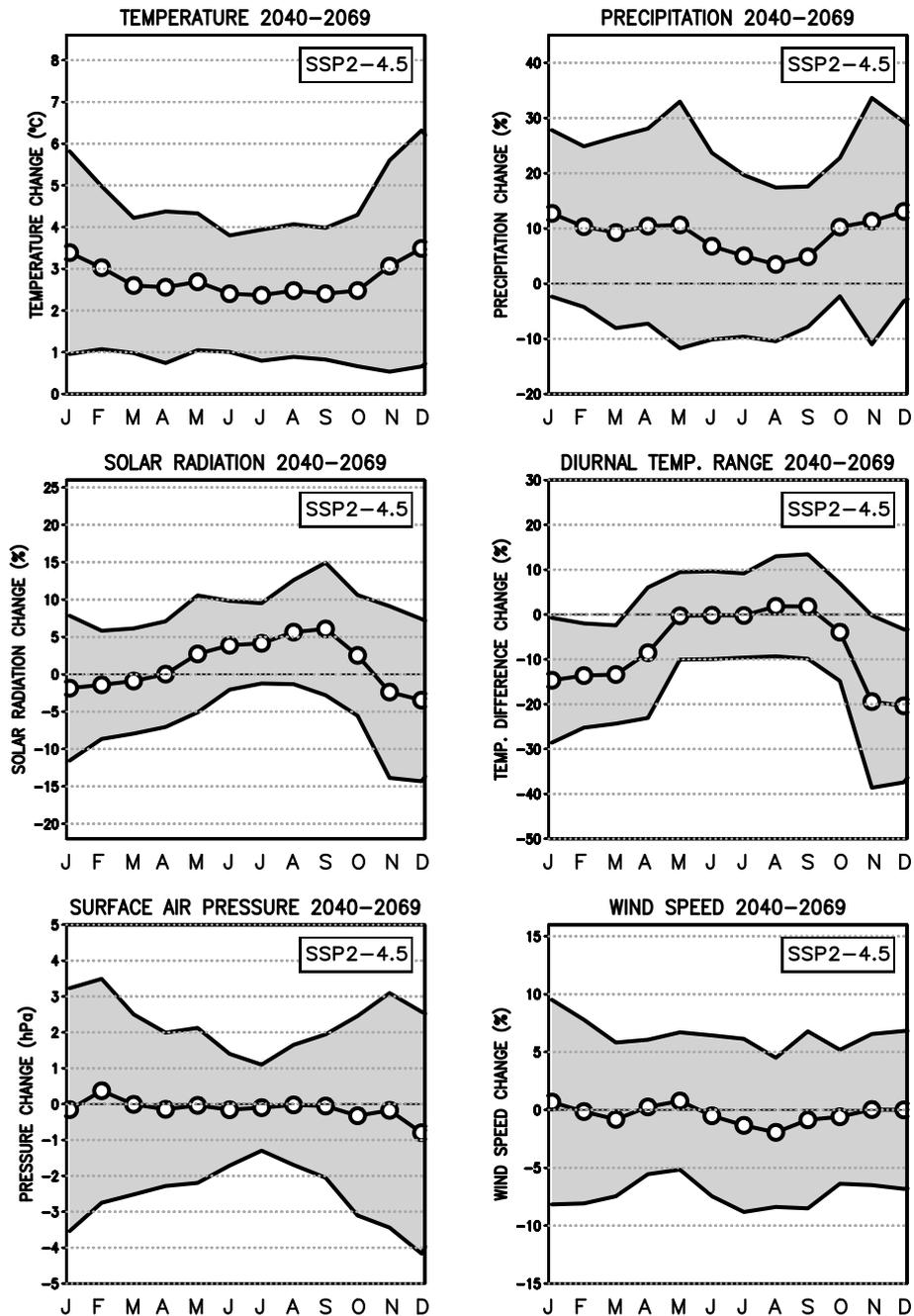
Fig. 6: Projected changes in the mean surface air temperature (in °C, top left), precipitation (in %, top right), incident solar radiation (in %, middle left), diurnal temperature range (in %, middle right), surface air pressure reduced to the sea level (in hPa, bottom left) and wind speed (in %, bottom right) in Finland under the SSP2-4.5 scenario for the period 2040–2069, relative to 1981–2010. The multi-model mean projections for every calendar month (J = January, F = February, ...), derived from the simulations performed with 19–28 GCMs (see Table 1), are denoted by open circles. Grey shading reveals the 90 % uncertainty intervals for the change.
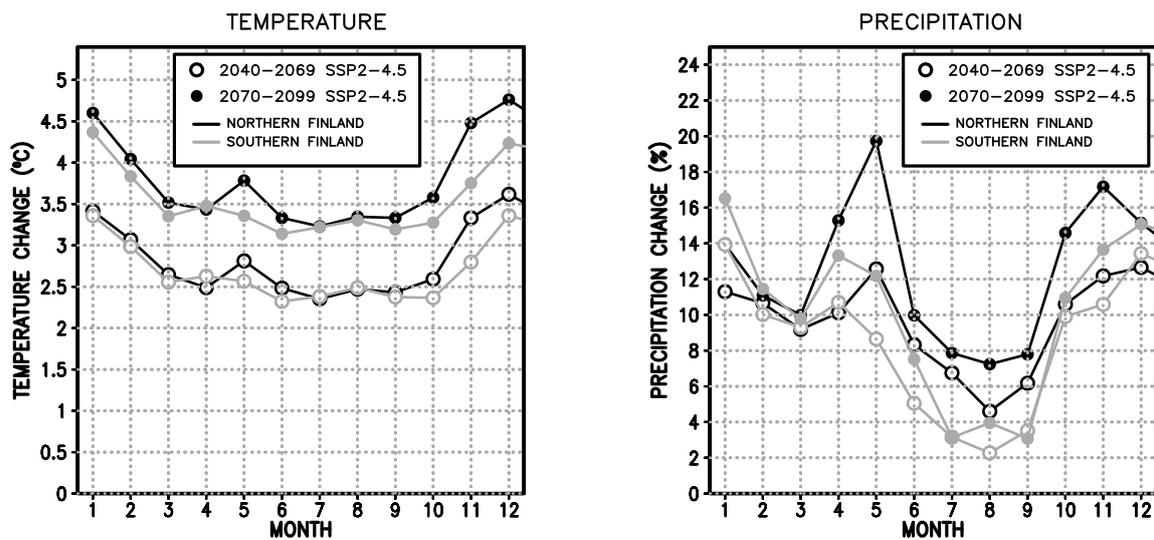
Fig. 7: Projected monthly multi-model mean changes in the surface air temperature (in °C, left panel) and precipitation (in %, right panel) in northern (black curves) and southern Finland (grey curves) for the periods 2040–2069 (open circles) and 2070–2099 (closed circles) relative to 1981–2010 under SSP2-4.5.

ondly, in the model output files relative humidity is expressed relative to ice in sub-zero temperatures, and several GCM output files contain substantial supersaturations in cold temperatures. It is unclear to what extent such supersaturations are plausible. On the other hand, the ensemble also includes many GCMs in which humidities exceeding 100 % have been truncated before publishing the output data. For consistency, we have truncated supersaturations from all the output data prior to calculating the projection. This ambiguity affects northern Finland more severely than the south, and therefore we have not calculated national spatial averages for humidity but only explore the projections at two discrete grid points (Fig. 8).

According to the multi-model mean, in the southernmost areas of Finland relative humidity is projected to decline by $\sim$ 1–2 % in all seasons apart from late autumn (Fig. 8, left panel). In the north, decreases only occur in summer and late spring (Fig. 8, right panel). As for many other variables, the inter-model spread is sizeable, and the sign of change cannot be established.

For assessing the sensitivity, we also calculated the relative humidity projections without performing any truncation of supersaturations. From March to November, the outcome was virtually identical to that shown in Fig. 8, while in the winter months the resulting decrease was slightly larger. As expected, the impact is largest in the north. These findings are in accordance with the fact that significant supersaturations only occur when the temperature is far below 0 °C.

The joint distributions of the modelled temperature responses and the corresponding changes in precipitation, solar radiation and the diurnal temperature range in the individual GCMs are shown in Fig. 9. The diagrams confirm the notion of quite a large spread
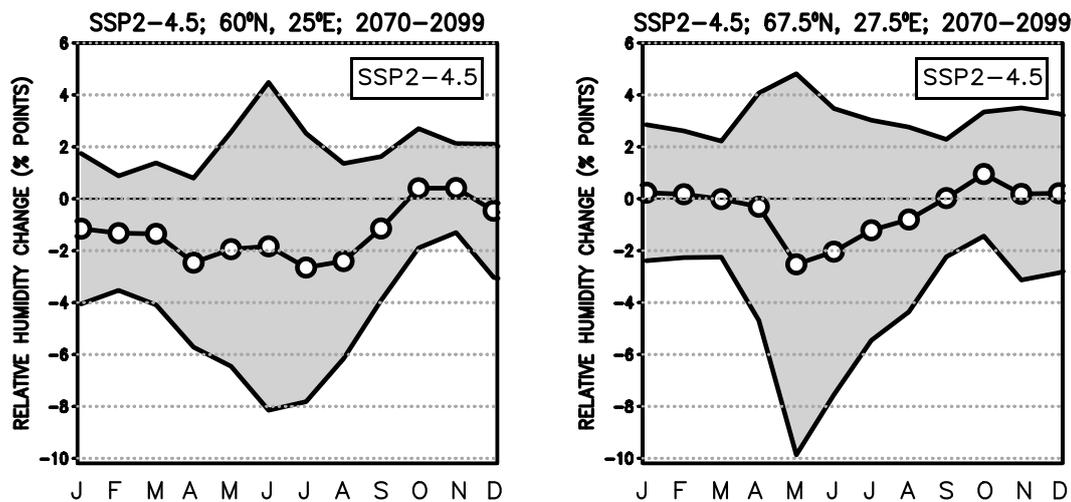
Fig. 8: Projected changes in relative humidity (in percent points) at 60°N, 25°E (left) and 67.5°N, 27.5°E (right) under the SSP2-4.5 scenario for the period 2070–2099. Supersaturations (RH > 100 %) relative to ice in the model output files have been truncated prior to the calculation of the projection. For further information, see the caption of Fig. 6.

among the modelled responses. For example, under SSP2-4.5 in winter, the modelled changes range from 1.4 °C to 7.5 °C for temperature, from 2 to 27 % for precipitation, from −13 to +12 % for solar radiation and from −36 to −8 % for the diurnal temperature range. Changes simulated by the individual GCMs are listed in Tables S7 and S8 of the Supplement. The joint distributions reveal that in winter, there is a positive dependence between the modelled temperature and precipitation changes, while changes in solar radiation and diurnal temperature range correlate negatively with the temperature responses. In summer, changes in temperature and precipitation are mutually uncorrelated, while solar radiation and the diurnal temperature range tend to increase most strongly in those models that simulate large warming. The signs of all the correlations are similar to those depicted in Fig. 9 of RJK16; for physical interpretation, see section 3.1 of that paper.

3.3   Geographical distributions of changes

Spatial distributions of changes in four climate variables in Europe by the mid-century period, separately for the winter and summer seasons, are shown in Figs. 10–13. In a qualitative sense, the spatial patterns of the responses are very similar to the corresponding patterns derived previously from the CMIP5 GCM data (Figs. 5–8 of RJK16). However, as the responses are forced by SSP2-4.5 here and by RCP8.5 in RJK16, the present changes are thoroughly weaker than the previous ones. As an exception, the positive solar radiation response in wide areas of the European continent in summer is now somewhat larger than previously. A potential explanation for the year-round increase in
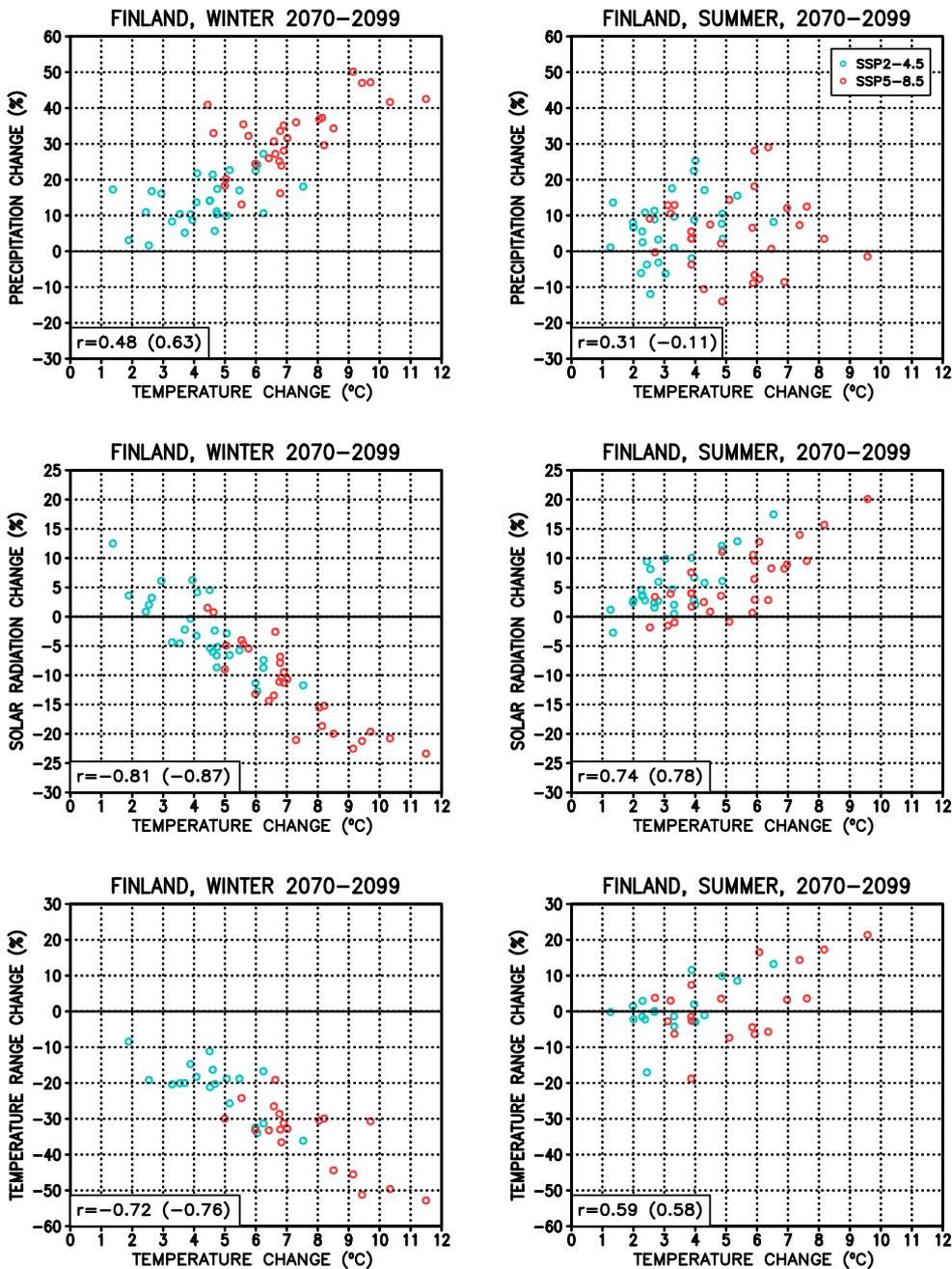
Fig. 9: Simulated changes of temperature from 1981–2010 to 2070–2099, in conjunction with corresponding changes in precipitation (top), incident solar radiation (middle) and diurnal temperature range (bottom) in Finland for the individual models. Bivariate distributions for December-February are depicted on the left, those for June-August on the right; model simulations under SSP2-4.5 are marked by blue and those under SSP5-8.5 by red symbols. The correlation coefficients between the responses in the two variables under SSP2-4.5 (and for SSP5-8.5 in parentheses) are given at the bottom-left corner. Correlations higher than 0.37 (0.48) are significant at the 5 % level and those exceeding 0.48 (0.58) at the 1 % level when data are available from 28 (19) GCMs.

the solar radiation response compared to the CMIP5 ensemble is that dimming caused by aerosol particles may be weaker in the present model simulations than in the previous ones. However, this idea cannot be verified by solely studying the model output files included in the present work. For the spatial averages of Finland, a more detailed comparison between the present and previous projections is shown in section 4.
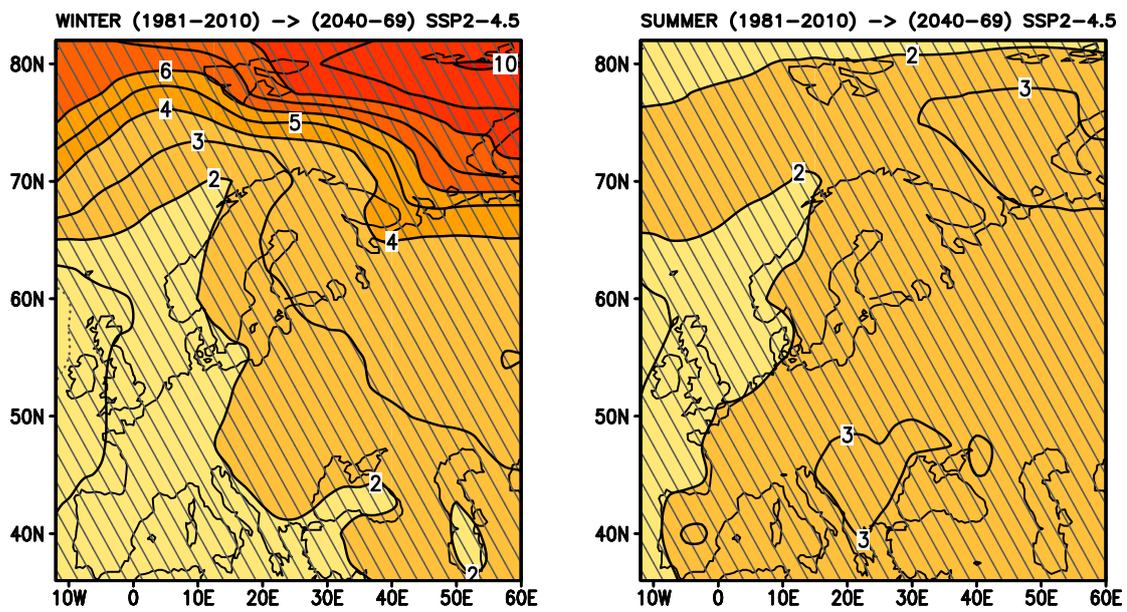

Fig. 10: Multi-model mean changes in the mean surface air temperature (in °C) in Europe in the December-February (left) and June-August (right) seasons under the SSP2-4.5 scenario for the period 2040–2069, relative to 1981–2010; an average of the simulations performed with the 28 GCMs listed in Table 1. Areas where more than 75 % of the models agree on the sign of change are hatched (for temperature, this condition is fulfilled over nearly the entire domain).

According to Fig. 10, temperatures increase everywhere over the domain, and the inter-model agreement is high. In winter, the largest warming occurs in the Arctic Ocean area, in summer in south-eastern Europe as well. Winter precipitation increases everywhere apart from the Mediterranean area in winter, while in summer there is a minor increase only to the north of 60°N (Fig. 11). In some areas of southern Europe, summer precipitation is projected to be reduced by ∼ 20 %. Solar radiation declines in northern ocean areas by up to 15 %, but over the European continent, radiation mainly increases (Fig. 12). In winter in the south-east and in summer over the majority of the continent, the increase is larger than 5 %. The diurnal temperature range generally decreases in winter, apart from the southernmost Europe; in summer, decreases are projected for oceans and small increases for the continent (Fig. 13). The decrease is substantial, 10 to 40 %, in northern and eastern Europe in winter and in the northern ocean areas throughout the year. The large decreases in diurnal temperature range over northern oceans evidently stem from the retreat of sea ice that has acted as a thermal insulator between the sea water and atmosphere in the baseline climate.
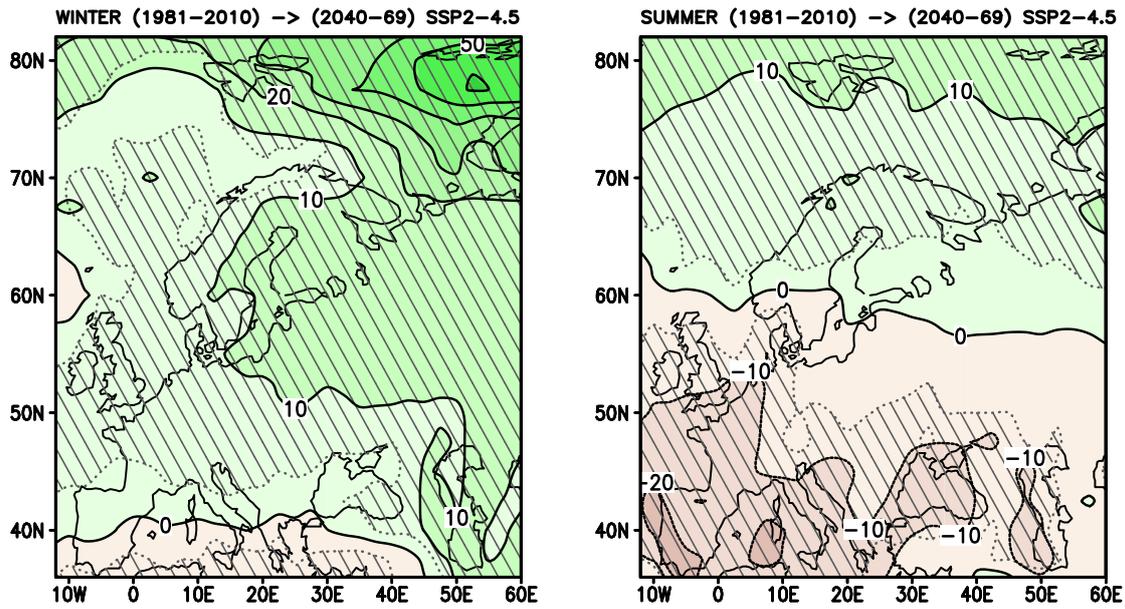
Fig. 11: Projected changes in precipitation (in %) in December-February (left) and June-August (right) under the SSP2-4.5 scenario; for more information, see the caption of Fig. 10.
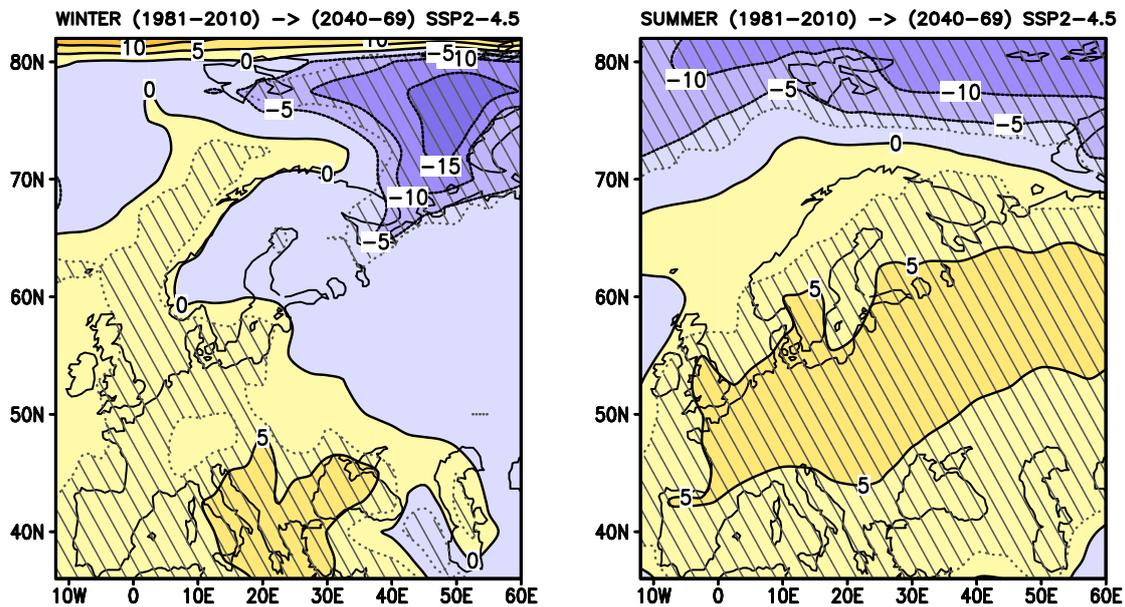
Fig. 12: Projected changes in incident solar radiation at the surface (in %) in December-February (left) and June-August (right) under the SSP2-4.5 scenario; for more information, see the caption of Fig. 10.

For precipitation, solar radiation and the diurnal temperature range, in wide areas more than 75 % of the GCMs agree on the sign of change, with the exception of the zones close to the contour of zero change.
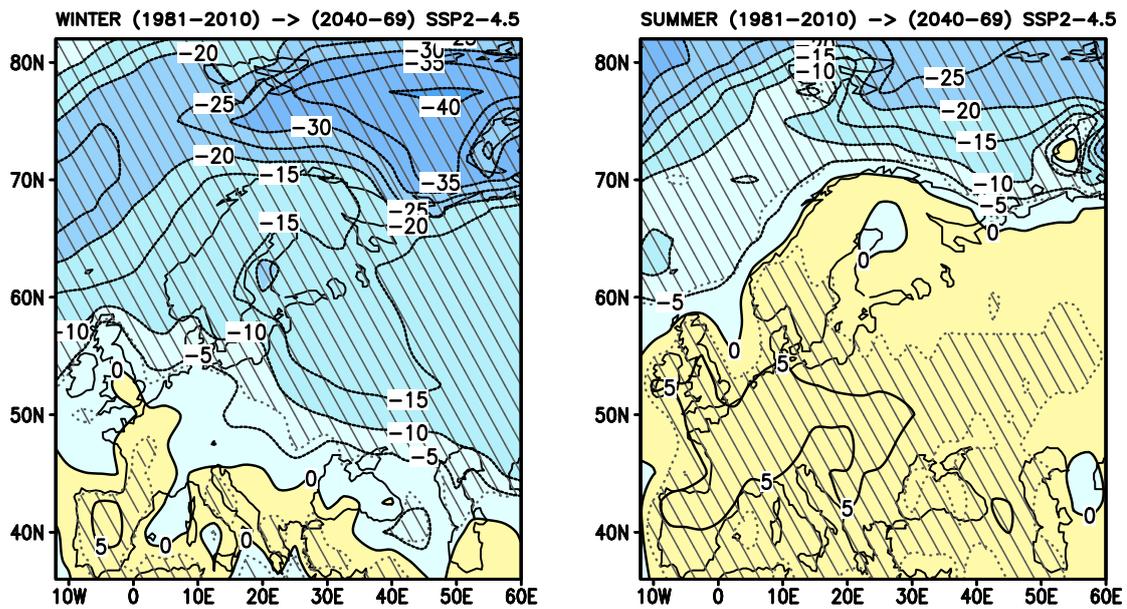
Fig. 13: Projected changes in the diurnal temperature range (T_{max}–T_{min}) (in %) in December-February (left) and June-August (right) under the SSP2-4.5 scenario; a mean of 19 GCMs. For more information, see the caption of Fig. 10.

Figs. S3–S6 show the geographical distributions of changes for the late-century period 2070–2099. The patterns are qualitatively similar to those in Figs. 10–13, but the amplitudes of changes are larger, in concordance with the stronger forcing in that period.

Relative humidity is likely to decrease in summer (Fig. S7). Over central and southern Europe, the decrease is substantial, amounting to 4–6 percentage points by 2040–2069. Potential changes in humidity in winter are not explored here owing to the ambiguity related to the supersaturation issue discussed in section 3.2.

Note that changes projected for the various climate quantities are physically consistent. In southern and central Europe in summer, all indicators show changes towards more arid conditions: precipitation and relative humidity decrease while solar radiation and the diurnal temperature range tend to amplify. Conversely, northern European climate becomes wetter in winter, with increasing precipitation and decreasing radiation and temperature range.

4   Comparison with the projections produced by the previous GCM generations

4.1   Differences between the projections derived from CMIP5 and CMIP6 GCMs

The present monthly projections of the mean temperature, precipitation and solar radiation for Finland are compared with their counterparts derived from the previous-generation CMIP5 GCMs in Fig. 14. To obtain the most robust potential signal, the late-century period 2070–2099 is considered. The forcing scenarios, SSP2-4.5 and RCP4.5,

are not wholly identical (*Meinshausen et al.*, 2020), but the nominal radiative forcing is the same. Consequently, differences between the projections mainly reflect dissimilarities in the models belonging to the two ensembles. According to the CMIP5 multi-model mean response to RCP4.5, the global-mean temperature increase from 1981–2010 to 2070–2099 was 1.85 °C (*Ruosteenoja et al.*, 2016a). The corresponding response to SSP2-4.5 derived from the present CMIP6 ensemble is 2.29 °C, i.e., 0.44 °C higher than the previous estimate.
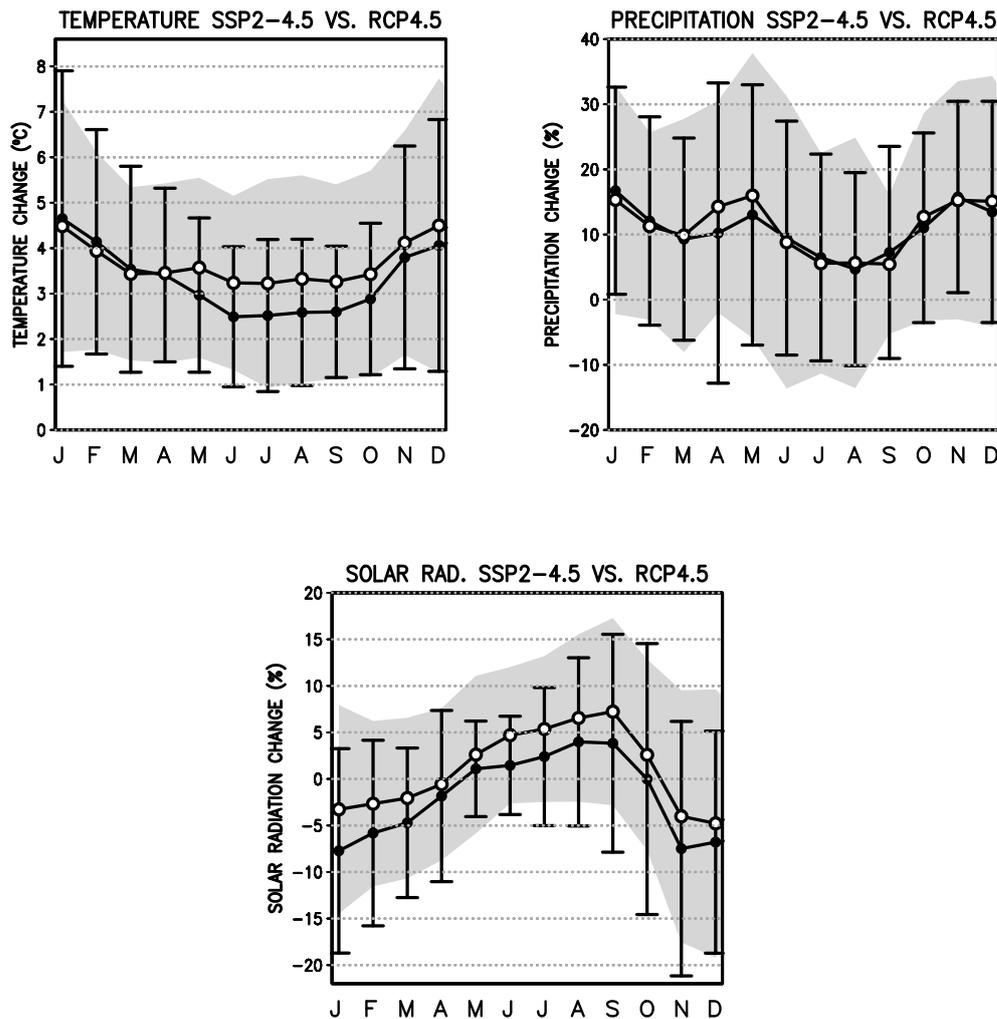
Fig. 14: Comparison of the projected monthly changes for Finland between the new CMIP6 and old CMIP5 simulations for the period 2070–2099, relative to 1981–2010: mean temperature (in °C, upper left), precipitation (in %, upper right) and incident solar radiation (in %, bottom). The multi-model mean projections for the calendar months (J = January, F = February, ...) are given for RCP4.5 (28 CMIP5 GCMs; closed circles) and SSP2-4.5 (28 CMIP6 GCMs; open circles). The 90 % uncertainty intervals for the change, analogous to those depicted in Fig. 6, are marked by grey shading for SSP2-4.5 and vertical bars for RCP4.5.

Temperature projections produced by the two model generations (Fig. 14, upper left panel) are nearly identical in the cold season from November to April. In the warm season

from June to September, the CMIP6 GCMs tend to warm the Finnish climate to a greater extent than the CMIP5 GCMs did, the difference in the late 21st century being about 0.7 °C. Even so, compared to the inter-SSP scenario differences or, in particular, inter-model scatter in warming, this difference is not very large. For example, according to the CMIP5 GCMs under RCP4.5, summer (June–August) temperatures were projected to increase by 2.5 (1.0–4.0) °C (Table S1 of RJK16); according to Table S1 of the present work, the corresponding temperature increases are 3.3 (1.2–5.3) °C under SSP2-4.5 and 2.2 (0.5–4.0) °C under SSP1-2.6.

For precipitation (Fig. 14, upper right panel), projections derived from the two model generations are very similar, regarding both the multi-GCM mean and inter-GCM scatter. Conversely, the incident solar radiation projection (Fig. 14, lower panel) has become 'brighter' throughout the year, the difference between the GCM generations being 1–4 percentage points. This indicates that the projected darkening of winters is now less severe and brightening of summers stronger than in the previous estimates.

For the wind speed and surface air pressure reduced to the sea level, the multi-model mean changes are close to zero according to both model generations (Figs. 6 and Fig. 3 of RJK16). Inter-GCM scatter in the wind-speed projections has been reduced because of the omission of the anomalously-behaving GFDL-ESM4 model (see section 2.2). Changes in the diurnal temperature range have remained nearly the same as previously (compare Tables S4 in the current work and RJK16).

Revealing the causes for the GCM-generation induced differences in the projected changes would require a profound scrutiny of the structure and parameterizations of all the GCMs belonging to both generations, and has thereby to be left beyond the scope of the present investigation. Moreover, as stated above, the two forcing scenarios (RCP4.5 and SSP2-4.5) are not quite identical but there are differences in the evolution of individual forcing agents.

4.2   CMIP6 versus early GCM generations

For future changes in two basic climatic variables, seasonal mean temperature and precipitation, national scenarios for Finland have been available since the 1990s. Nevertheless, the number of GCMs from which the climate scenarios have been derived has increased greatly in time: from a few (*Carter et al.*, 1996) to almost 30 (RJK16 and the present paper). In all the consecutive climate scenarios, at least three alternative pathways of global greenhouse gas emissions have been taken into account. Four out of these five sets of climate projections considered either the SRES B1 (*Jylhä et al.*, 2009, 2004), RCP4.5 (RJK16) or SSP2-4.5 scenario (this paper). As discussed in RJK16 and section 4.1 of the present paper, in all three scenarios the future evolution of radiative forcing is similar enough to enable comparisons between the corresponding multi-model mean responses produced by the various GCM generations.

The SRES B1 scenario was included both in the projections constructed by *Jylhä et al.* (2004) and *Jylhä et al.* (2009), but the studies utilized data from different GCM generations. The first work analysed output data from six GCMs that contributed to the

Third Assessment Report of IPCC, and the second one examined 19 CMIP3 GCMs contributing to the next report. Because of the small number of GCMs in *Jylhä et al.*, 2004, the results are far less robust than the more recent national climate scenarios for Finland. This holds both for the reported multi-model mean projections and uncertainty intervals for the changes. Instead of considering the 90 % uncertainty intervals of the change, in this case the difference between the models giving the weakest and strongest response was calculated, since fitting a normal distribution to a six-member ensemble would not have been justifiable. Therefore, the uncertainty ranges reported by *Jylhä et al.* (2004) should be regarded as rudimentary.

The multi-model mean projections of the seasonal and annual mean temperature and precipitation produced by the various GCM generations, in conjunction with the related uncertainty intervals, are shown in Fig. 15. Instead of giving absolute changes between a baseline and future period, like elsewhere in this paper, the results now denote changes per decade by the period 2070–2099. In practice, this overturns the minor influence of the slightly divergent baseline periods used in the various studies in calculating the trends. It can be seen that for summer and autumn, as well as for the annual average, the projected multi-model mean warming has intensified across the consecutive generations. Conversely, the inter-generation differences in the rate of wintertime warming are small. As well, considering the wide uncertainty intervals, the multi-model mean projections for precipitation produced by the four model generations diverge rather little.

The first set of climate scenarios for Finland, built by *Carter et al.* (1996), adopted three alternative greenhouse gas scenarios that had been published in 1992. Radiative forcing in SRES B1 falls between the two lowest alternatives but is not very close to either of them. Therefore, we did not include the early results of *Carter et al.* (1996) in Fig. 15. Even so, it is worth noting that the central estimates for warming provided in that work, ranging from $0.3\,°\mathrm{C}/10\,\mathrm{a}$ in summer to $0.6\,°\mathrm{C}/10\,\mathrm{a}$ winter, are fairly close to the present projections: about $0.5\,°\mathrm{C}/10\,\mathrm{a}$ in winter and $0.4\,°\mathrm{C}/10\,\mathrm{a}$ in other seasons (supplement Table S1).
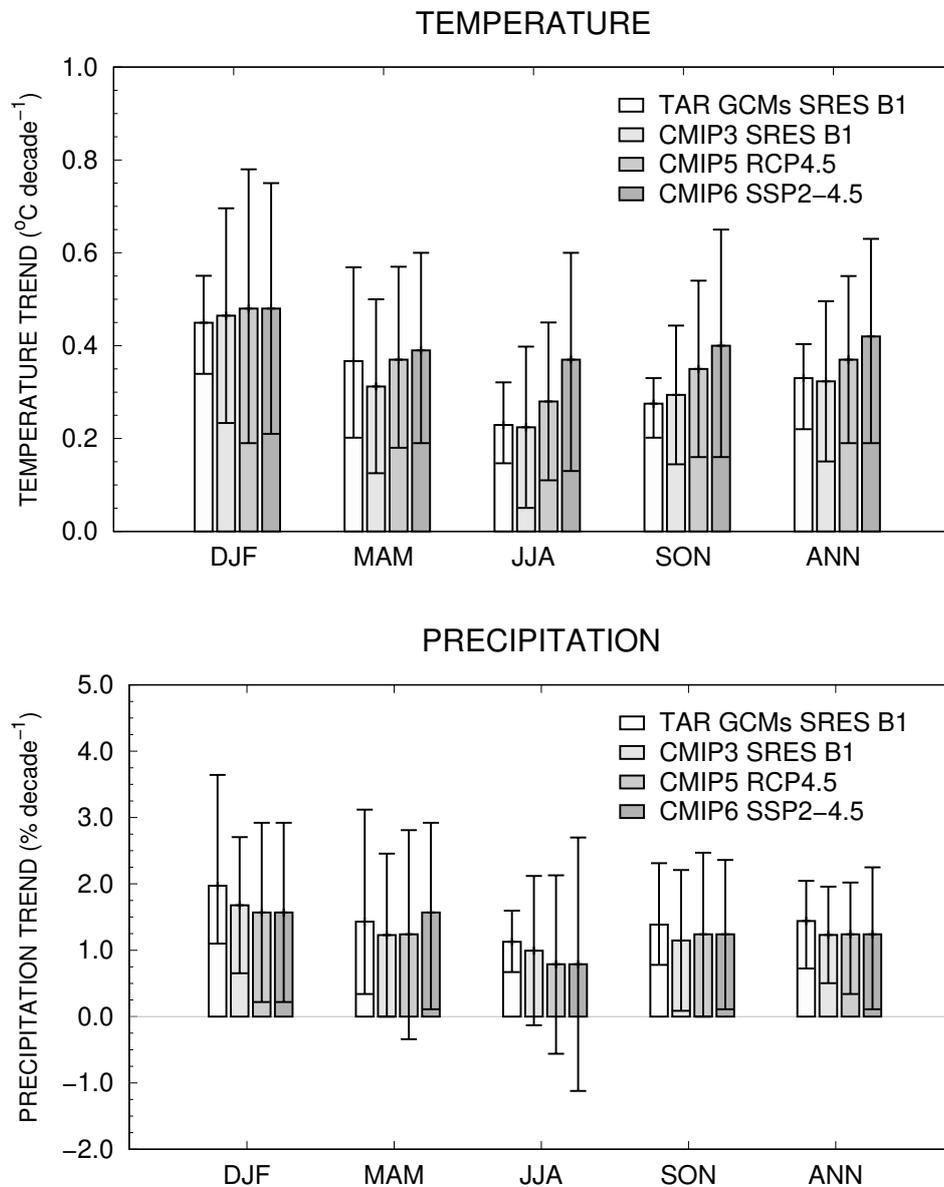
TEMPERATURE

PRECIPITATION

Fig. 15: Comparison of projected trends in seasonal (DJF: winter, MAM: spring, JJA: summer, SON: autumn) and annual mean temperatures (in °C decade^{-1}; upper panel) and precipitation (in % decade^{-1}; lower panel) in Finland by the end of this century. The following GCM ensembles and corresponding greenhouse gas scenarios are examined (columns from left to right): six GCMs under SRES B1, contributing to the IPCC Third Assessment Report (TAR); 19 CMIP3 GCMs under SRES B1; 28 CMIP5 GCMs under RCP4.5; and 28 CMIP6 GCMs under SSP2-4.5. The vertical bars depict the multi-model mean projections and whiskers uncertainty intervals for the change (see text for details). The baseline periods used for TAR was 1961–1990, for CMIP3 1971–2000 and for CMIP5–6 1981–2010. The CMIP3 results are downloadable from `https://www.ilmatieteenlaitos.fi/lampotila-sres-b1` and `https://www.ilmatieteenlaitos.fi/sademaara-sres-b1`.

5   Summary and conclusions

It is inevitable that warming continues in Finland during the next few decades (Fig. 2). Even under the lowest-emission scenario examined (SSP1-2.6), we have to prepare ourselves for a larger than 2 °C warming in our country relative to baseline period 1981–2010 by the late 21st century. Compared to the current Finnish conditions (early 2020s), this corresponds to additional warming of about one degree.

Nevertheless, it is quite possible and perhaps even likely that, by the end of this century, the annual mean temperature in Finland will be 2 °C to 3 °C higher than presently (SSP2-4.5). If the measures to curtail global greenhouse gas emissions fail altogether, warming will be even more severe. According to all forcing scenarios, warming is likely to be stronger in winter than in summer, even though the projected seasonal contrast in the temperature increase has diminished to some extent compared with the previous model generations. If the multi-model mean warming under SSP2-4.5 were realized, in the 2080s central Finland would experience a temperature climate somewhat similar to that in south-eastern Byelorussia in 1981–2010. Of course, this does not indicate that all the characteristics of climate would be similar.

Contemporaneously, the precipitation totals are likely to increase, even though in southern Finland in summer, the multi-model mean change appears to be negligibly small. Solar radiation presumably slightly increases in summer and decreases in winter. Differences between the daily maximum and minimum temperatures tend to decrease in winter and remain virtually unchanged in summer. In the mean wind speed, the projected changes are minor. Accordingly, despite the expectable significant changes in temperatures, some features of the Finnish climate may remain nearly unaltered.

All the projected changes are subject to substantial inter-model spread. Nevertheless, it is virtually certain that the mean temperatures increase throughout the year and the diurnal temperature range is reduced in winter. Furthermore, there is quite a high probability that the precipitation totals increase in winter and incident solar radiation in summer. In any case, considering the large inter-model scatter in the projections, all the decisions concerning adaptation to changing climate have inevitably to be inferred from somewhat uncertain climate information. In addition, uncertainties related to the success/failure of climate policy become increasingly important in the second half of the ongoing century.

Taking into account the recent advances in climate policy, this paper mainly focusses on the medium-level SSP2-4.5 greenhouse gas scenario. Therefore, the changes depicted in Figs. 6 and 10–13, for instance, are generally weaker than those reported in RJK16 in which the high-emission RCP8.5 scenario was predominantly examined. Nonetheless, when one uses an analogous forcing scenario for both the CMIP5 and CMIP6 ensembles (RCP4.5 versus SSP2-4.5), summertime warming conversely appears to have become stronger than previously. Even so, this might at least partly be an artifact since *Stolpe et al.* (2021) state that the recent CMIP6 GCMs in general to some extent tend to overestimate global warming as a function of forcing. The previous CMIP5 GCMs as a collective were more realistic in this respect. It is interesting to note that summer-season warming has intensified even more strongly when compared with the model generations older than

CMIP5 (Fig. 15).

When examining the entire European continent, warming is projected to be strongest in the south-east in summer and in the north-east in winter. According to the multi-model mean projection, precipitation increases in the north and decreases in the south; in central Europe, a decrease is projected for summer and an increase for winter. Incident solar radiation increases throughout the continent in summer and in the south and west in winter.

As shown in R21 (e.g., Figs. 9–12 of the report), the outcome of the GCM simulations always differs more or less from the observed climate. Hence, modelled values as such should never be employed to represent the present or future climate. For techniques to tackle this issue, delta change methods and bias correction, see section 4 of RJK16 and references therein.

From a narrow Finnish perspective only, the change will entail both positive and negative consequences; a few examples are given here. Growing seasons in agriculture will become longer and warmer, allowing farming of new crops and cultivars (*Peltonen-Sainio and Jauhiainen*, 2020), but this benefit is counteracted by the invasion of new pests, plant diseases and weeds (*Hakala et al.*, 2011). Analogously, in forests higher temperatures tend to promote growth but the risk for biotic damages by new pests and pathogens increases (*Venäläinen et al.*, 2020). Moreover, conditions of both forestry and agriculture are affected by increasing occurrence of drought in summer, particularly in southern Finland. The number of forest fires is projected to increase substantially (*Lehtonen et al.*, 2016b).

Human deaths due to cold weather are likely to be reduced while heat-induced mortality increases (*Gasparrini et al.*, 2017; *Ruuhela et al.*, 2018). Dark winters (*Ruuhela et al.*, 2009) and climate anxiety (*Hickman et al.*, 2021) may bring about mental health problems. As well, it is possible that climate-induced migration (e.g., *Grecequet et al.*, 2017) increases. In buildings, the need for warming energy is reduced (*Jylhä et al.*, 2015) but there is an increasing risk for uncomfortably high summertime indoor temperatures (*Velashjerdi Farahani et al.*, 2021) and reduced moisture safety (*Pakkala*, 2020; *Viljanen et al.*, 2020).

Information about the anticipated future climatic changes under the SSP scenarios supports development of strategies for adaptation to climate change, e.g., updates for the report of *Gregow et al.* (2021). For example, high summer-time temperatures pose a significant risk to health for vulnerable people even in the current-day climate (*Kollanus et al.*, 2021), and, as stated above, the situation will be exacerbated as a consequence of the projected warming. State-of-the-art climate scenarios constitute the basis for cost-effective and socially acceptable solutions for adaptation. In many applications, creating adequately detailed scenarios requires the datasets for future climate to be represented at a daily or even hourly level. An example of how hourly weather data can be elaborated by using an delta-change approach is provided by *Jylhä et al.* (2020).

In the global perspective, the projected climatic changes are predominantly detrimental. Numerous plant and animal species are threatened by extinction. In many countries in the third world, living conditions may deteriorate considerably, causing major hu-

man suffering and potentially extensive climate-induced migration. An unabated climate change would make the world hazardous for the whole mankind. Accordingly, considering all the negative global impacts of climate change, a prudent climate policy benefits Finland as well as the entire world.

Acknowledgments

References

Aalto, J., P. Pirinen and K. Jylhä, 2016. New gridded daily climatology of Finland: Permutation-based uncertainty estimates and temporal trends in climate. *Journal of Geophysical Research — Atmospheres*, **121**, 3807–3823. DOI: `10.1002/2015JD024651`.

Carter, T. R., M. Posch and H. Tuomenvirta, 1996. The SILMU scenarios: specifying Finland's future climate for use in impact assessment. *Geophysica*, **32**, 235–260.

Eklund, A., J. A. Mårtensson, S. Bergström, E. Björck, J. Dahné, L. Lindström, D. Nordborg, J. Olsson, L. Simonsson and E. Sjökvist, 2015. Sveriges framtida klimat (Sweden's future climate). Klimatologi 14. In Swedish, with abstract in English. Sveriges meteorologiska och hydrologiska institut, 94. URL: `https://www.smhi.se/en/publications/sweden-s-future-climate-1.89858`.

Eyring, V., S. Bony, G. A. Meehl, C. A. Senior, B. Stevens, R. J. Stouffer and K. E. Taylor, 2016. Overview of the Coupled Model Intercomparison Project Phase 6 (CMIP6) experimental design and organization. *Geoscientific Model Development*, **9**, 1937–1958. DOI: `10.5194/gmd-9-1937-2016`.

Fortelius, C., E. Holopainen, J. Kaurola, K. Ruosteenoja and J. Räisänen, 1996. "Climate models and scenarios". In: *The Finnish Research Programme on Climate Change (SILMU), Final Report*. Ed. by J. Roos. Vol. 4/96. Publications of the Academy of Finland, 43–49.

Gasparrini, A., Y. Guo, F. Sera, A. M. Vicedo-Cabrera, V. Huber, S. Tong, M. de Sousa Zanotti Stagliorio Coelho, P. Hilario Nascimento Saldiva, E. Lavigne, P. Matus Correa, N. Valdes Ortega, H. Kan, S. Osorio, J. Kyselý, A. Urban, J. J. K. Jaakkola, N. R. I. Ryti, M. Pascal, P. G. Goodman, A. Zeka, P. Michelozzi, M. Scortichini, M. Hashizume, Y. Honda, M. Hurtado-Diaz, J. Cesar Cruz, X. Seposo, H. Kim, A. Tobias,

C. Iñiguez, B. Forsberg, D. O. Åström, M. S. Ragettli, Y. L. Guo, C. Wu, A. Zanobetti, J. Schwartz, M. L. Bell, T. Ng. Dang, D. D. Van, C. Heaviside, S. Vardoulakis, S. Hajat, A. Haines and B. Armstrong, 2017. Projections of temperature-related excess mortality under climate change scenarios. *The Lancet Planetary Health*, **1**, e360–e367. DOI: 10.1016/S2542-5196(17)30156-0.

Giorgi, F., E. Coppola, C. Teichmann and D. Jacob, 2021. Editorial for the CORDEX-CORE Experiment I Special Issue. *Climate Dynamics*, **57**, 1265–1268. DOI: 10.1007/s00382-021-05902-w.

Grecequet, M., J. DeWaard, J. J. Hellmann and Guy J. Abel, 2017. Climate Vulnerability and Human Migration in Global Perspective. *Sustainability*, **9**. DOI: 10.3390/su9050720.

Gregow, H., A. Mäkelä, H. Tuomenvirta, S. Juhola, J. Käyhkö, A. Perrels, E. Kuntsi-Reunanen, I. Mettiäinen, K. Näkkäläjärvi, J. Sorvali, H. Lehtonen, M. Hildén, N. Veijalainen, H. Kuosa, M. Sihvonen, U. Leijala, S. Ahonen, M. Johansson, J. Haapala, H. Korhonen, M. Ollikainen, S. Lilja, R. Ruuhela, S. Rasmus, J. Särkkä and S-M. Siiriä, 2021. Ilmastonmuutokseen sopeutumisen ohjauskeinot, kustannukset ja alueelliset ulottuvuudet. Raportti 2/2021. (In Finnish, with abstracts in Swedish, Saami, and English). Suomen ilmastopaneeli. URL: https://www.ilmastopaneeli.fi/wp-content/uploads/2021/09/SUOMI-raportti%5C_final.pdf.

Hakala, K., A. O. Hannukkala, E. Huusela-Veistola, M. Jalli and P. Peltonen-Sainio, 2011. Pests and diseases in a changing climate: a major challenge for Finnish crop production. *Agricultural and Food Science*, **20**, 3–14.

Hanssen-Bauer, I., E. J. Førland, I. Haddeland, H. Hisdal, S. Mayer, A. Nesje, J. E. Ø. Nilsen, S. Sandven, A. B. Sandø, A. Sorteberg and B. Ådlandsvik, 2017. Climate in Norway 2100 – a knowledge base for climate adaptation. NCCC Report 1/2017. Oslo, Norway: Norwegian Centre for Climate Services.

Hickman, C., E. Marks, P. Pihkala, S. Clayton, R. E. Lewandowski, E. E. Mayall, B. Wray, C. Mellor and L. van Susteren, 2021. Climate anxiety in children and young people and their beliefs about government responses to climate change: a global survey. *The Lancet Planetary Health*, **5**, e863–e873. DOI: 10.1016/S2542-5196(21)00278-3.

IPCC, 2021. *Climate Change 2021: The Physical Science Basis. Contribution of Working Group I to the Sixth Assessment Report of the Intergovernmental Panel on Climate Change*. [Masson-Delmotte, V., P. Zhai, A. Pirani, S.L. Connors, C. Péan, S. Berger, N. Caud, Y. Chen, L. Goldfarb, M.I. Gomis, M. Huang , K. Leitzell, E. Lonnoy, J.B.R. Matthews , T.K. Maycock, T. Waterfield, O. Yelekçi , R. Yu and B. Zhou (eds.)] Cambridge University Press.

Jaagus, J. and K. Mändla, 2014. Climate change scenarios for Estonia based on climate models from the IPCC Fourth Assessment Report. *Estonian Journal of Earth Sciences*, **63**, 166–180. DOI: 10.3176/earth.2014.15.

Jokinen, P., P. Pirinen, J.-H. Kaukoranta, A. Kangas, P. Alenius, P. Eriksson, M. Johansson and S. Wilkman, 2021. Tilastoja Suomen ilmastosta ja merestä 1991–2020 (Climatological and oceanographic statistics of Finland 1991–2020). Reports 2021:8. (In

Finnish, with abstracts in Swedish and English). Finnish Meteorological Institute, 169. URL: https://helda.helsinki.fi/handle/10138/336063.

Jones, P. W., 1999. First- and Second-Order Conservative Remapping Schemes for Grids in Spherical Coordinates. *Monthly Weather Review*, **127**, 2204–2210. DOI: 10.1175/1520-0493(1999)127<2204:FASOCR>2.0.CO;2.

Jylhä, K., J. Jokisalo, K. Ruosteenoja, K. Pilli-Sihvola, T. Kalamees, T. Seitola, H. M. Mäkelä, R. Hyvönen, M. Laapas and A. Drebs, 2015. Energy demand for the heating and cooling of residental houses in Finland in a changing climate. *Energy and Buildings*, **99**, 104–116. DOI: 10.1016/j.enbuild.2015.04.001.

Jylhä, K., M. Laapas, K. Ruosteenoja, L. Arvola, A. Drebs, J. Kersalo, S. Saku, H. Gregow, H.-R. Hannula and P. Pirinen, 2014. Climate variability and trends in the Valkea-Kotinen region, southern Finland: comparisons between the past, current and projected climates. *Boreal Env. Res.*, **19 (suppl. A)**, 4–30.

Jylhä, K., K. Ruosteenoja, H. Böök, A. Lindfors, P. Pirinen, M. Laapas and A. Mäkelä, 2020. Nykyisen ja tulevan ilmaston säätietoja rakennusfysikaalisia laskelmia ja energialaskennan testivuotta 2020 varten (Weather data for building-physical studies and the building energy reference year 2020 in a changing climate). Raportteja 2020:6. (In Finnish with abstract in English and Swedish). Ilmatieteen laitos, 81. DOI: 10.35614/isbn.9789523361287.

Jylhä, K., K. Ruosteenoja, J. Räisänen, A. Venäläinen, H. Tuomenvirta, L. Ruokolainen, S. Saku and T. Seitola, 2009. Arvioita Suomen muuttuvasta ilmastosta sopeutumistutkimuksia varten — ACCLIM-hankkeen raportti 2009 (The changing climate in Finland: estimates for adaptation studies. ACCLIM project report 2009.) Reports 2009:4. (In Finnish, extended abstract also in English). Finnish Meteorological Institute, 102.

Jylhä, K., H. Tuomenvirta and K. Ruosteenoja, 2004. Climate change projections for Finland during the 21st century. *Boreal Env. Res.*, **9**, 127–152.

Kjellström, E., L. Bärring, G. Nikulin, C. Nilsson, G. Persson and G. Strandberg, 2016. Production and use of regional climate model projections – A Swedish perspective on building climate services. *Climate services*, **2–3**, 15–29. DOI: 10.1016/j.cliser.2016.06.004.

Kollanus, V., P. Tiittanen and T. Lanki, 2021. Mortality risk related to heatwaves in Finland – Factors affecting vulnerability. *Environmental Research*, **201**, 111503. DOI: 10.1016/j.envres.2021.111503.

Laapas, M. and A. Venäläinen, 2017. Homogenization and trend analysis of monthly mean and maximum wind speed time series in Finland, 1959–2015. *International Journal of Climatology*, **37**, 4803–4813. DOI: 10.1002/joc.5124.

Lehtonen, I., M. Kämäräinen, H. Gregow, A. Venäläinen and H. Peltola, 2016a. Heavy snow loads in Finnish forests respond regionally asymmetrically to projected climate change. *Natural Hazards and Earth System Sciences*, **16**, 2259–2271. DOI: 10.5194/nhess-16-2259-2016.

Lehtonen, I., A. Venäläinen, M. Kämäräinen, A. Asikainen, J. Laitila, P. Anttila and H. Peltola, 2019. Projected decrease in wintertime bearing capacity on different forest and

soil types in Finland under a warming climate. *Hydrology and Earth System Sciences*, **23**, 1611–1631. DOI: 10.5194/hess-23-1611-2019.

Lehtonen, I., A. Venäläinen, M. Kämäräinen, H. Peltola and H. Gregow, 2016b. Risk of large-scale fires in boreal forests of Finland under changing climate. *Natural Hazards and Earth System Sciences*, **16**, 239–253. DOI: 10.5194/nhess-16-239-2016.

Luomaranta, A., J. Aalto and K. Jylhä, 2019. Snow cover trends in Finland over 1961–2014 based on gridded snow depth observations. *International Journal of Climatology*, **39**, 3147–3159. DOI: 10.1002/joc.6007.

Meinshausen, M., Z. R. J. Nicholls, J. Lewis, M. J. Gidden, E. Vogel, M. Freund, U. Beyerle, C. Gessner, A. Nauels, N. Bauer, J. G. Canadell, J. S. Daniel, A. John, P. B. Krummel, G. Luderer, N. Meinshausen, S. A. Montzka, P. J. Rayner, S. Reimann, S. J. Smith, M. van den Berg, G. J. M. Velders, M. K. Vollmer and R. H. J. Wang, 2020. The shared socio-economic pathway (SSP) greenhouse gas concentrations and their extensions to 2500. *Geoscientific Model Development*, **13**, 3571–3605. DOI: 10.5194/gmd-13-3571-2020.

Mikkonen, S., M. Laine, H.M. Mäkelä, H. Gregow, H. Tuomenvirta, M. Lahtinen and A. Laaksonen, 2015. Trends in the average temperature in Finland, 1847–2013. English. *Stochastic Environmental Research and Risk Assessment*, **29** (6), 1521–1529. DOI: 10.1007/s00477-014-0992-2.

O'Neill, B. C., C. Tebaldi, D. P. van Vuuren, V. Eyring, P. Friedlingstein, G. Hurtt, R. Knutti, E. Kriegler, J.-F. Lamarque, J. Lowe, G. A. Meehl, R. Moss, K. Riahi and B. M. Sanderson, 2016. The Scenario Model Intercomparison Project (ScenarioMIP) for CMIP6. *Geoscientific Model Development*, **9**, 3461–3482. DOI: 10.5194/gmd-9-3461-2016.

Olsson, T., J. Jakkila, N. Veijalainen, L. Backman, J. Kaurola and B. Vehviläinen, 2015. Impacts of climate change on temperature, precipitation and hydrology in Finland – studies using bias corrected Regional Climate Model data. *Hydrology and Earth System Sciences*, **19**, 3217–3238. DOI: 10.5194/hess-19-3217-2015.

Pakkala, T., 2020. Assessment of the Climate Change Effects on Finnish Concrete Facades and Balconies. Tampere University Dissertations 204. Tampere University, Faculty of Built Environment, Finland. URL: https://urn.fi/URN:ISBN:978-952-03-1423-1.

Pakkala, T., A Köliö, J. Lahdensivu and M. Pentti, 2019. Predicted corrosion rate on outdoor exposed concrete structures. *International Journal of Building Pathology and Adaptation*, **37**, 679–698. DOI: 10.1108/IJBPA-11-2018-0086.

Peltonen-Sainio, P. and L. Jauhiainen, 2020. Large zonal and temporal shifts in crops and cultivars coincide with warmer growing seasons in Finland. *Regional Environmental Change*, **20**, 89. DOI: 10.1007/s10113-020-01682-x.

Peltonen-Sainio, P., T. Palosuo, K. Ruosteenoja, L. Jauhiainen and H. Ojanen, 2018. Warming autumns at high latitudes of Europe: an opportunity to lose or gain in cereal production? *Regional Environmental Change*, **18**, 1453–1465. DOI: 10.1007/s10113-017-1275-5.

Riahi, K., D. P. van Vuuren, E. Kriegler, J. Edmonds, B. C. O'Neill, S. Fujimori, N. Bauer, K. Calvin, R. Dellink, O. Fricko, W. Lutz, A. Popp, J. Crespo Cuaresma, K. C. Samir, M. Leimbach, L. Jiang, T. Kram, S. Rao, J. Emmerling, K. Ebi, T. Hasegawa, P. Havlik, F. Humpenöder, L. Aleluia Da Silva, S. Smith, E. Stehfest, V. Bosetti, J. Eom, D. Gernaat, T. Masui, J. Rogelj, J. Strefler, L. Drouet, V. Krey, G. Luderer, M. Harmsen, K. Takahashi, L. Baumstark, J. C. Doelman, M. Kainuma, Z. Klimont, G. Marangoni, H. Lotze-Campen, M. Obersteiner, A. Tabeau and M. Tavoni, 2017. The Shared Socioeconomic Pathways and their energy, land use, and greenhouse gas emissions implications: An overview. *Global Environmental Change*, **42**, 153–168. DOI: `10.1016/j.gloenvcha.2016.05.009`.

Ruosteenoja, K., 2021. Applicability of CMIP6 models for building climate projections for northern Europe. Reports 2021:7. Finnish Meteorological Institute, 48. DOI: `10.35614/isbn.9789523361416`.

Ruosteenoja, K., K. Jylhä and M. Kämäräinen, 2016a. Climate projections for Finland under the RCP forcing scenarios. *Geophysica*, **51**, 17–50.

Ruosteenoja, K., M. Kämäräinen, S. Aniskeviča, P. Pirinen and A. Mäkelä, 2016b. Development of climate change scenarios for Latvia for the period until the year 2100. Reports 2016:7. Finnish Meteorological Institute, 51.

Ruosteenoja, K. and J. Räisänen, 2021. Evolution of observed and modelled temperatures in Finland in 1901–2018 and potential dynamical reasons for the differences. *International Journal of Climatology*, **41**, 3374–3390. DOI: `10.1002/joc.7024`.

Ruosteenoja, K., J. Räisänen, K. Jylhä, H. Mäkelä, I. Lehtonen, H. Simola, A. Luomaranta and S. Weiher, 2013. Maailmanlaajuisiin CMIP3-malleihin perustuvia arvioita Suomen tulevasta ilmastosta (Climate change estimates for Finland on the basis of global CMIP3 climate models). Raportteja 2013:4. (In Finnish with abstracts in English and Swedish). Finnish Meteorological Institute, 83.

Ruosteenoja, K., T. Vihma and A. Venäläinen, 2019. Projected changes in European and North Atlantic seasonal wind climate derived from CMIP5 simulations. *Journal of Climate*, **32**, 6467–6490. DOI: `10.1175/JCLI-D-19-0023.1`.

Ruuhela, R., L. Hiltunen, A. Venäläinen, P. Pirinen and T. Partonen, 2009. Climate impact on suicide rates in Finland from 1971 to 2003. *International Journal of Biometeorology*, **53**, 167–175. DOI: `10.1007/s00484-008-0200-5`.

Ruuhela, R., O. Hyvärinen and K. Jylhä, 2018. Regional Assessment of Temperature-Related Mortality in Finland. *International Journal of Environmental Research and Public Health*, **15**. DOI: `10.3390/ijerph15030406`.

Saranko, O., C. Fortelius, K. Jylhä, K. Ruosteenoja, E. Brattich, S. Di Sabatino and V. Nurmi, 2020. Impacts of town characteristics on the changing urban climate in Vantaa. *Science of The Total Environment*, **727**, 138471. DOI: `10.1016/j.scitotenv.2020.138471`.

Sepp, M., T. Tamm and V. Sagris, 2018. The future climate regions in Estonia. *Estonian Journal of Earth Sciences*, **67**, 259–268. DOI: `10.3176/earth.2018.19`.

Stolpe, M. B., K. Cowtan, I. Medhaug and R. Knutti, 2021. Pacific variability reconciles observed and modelled global mean temperature increase since 1950. *Climate Dynamics*, **56**, 613–634. DOI: `10.1007/s00382-020-05493-y`.

Tietäväinen, H., H. Tuomenvirta and A. Venäläinen, 2010. Annual and seasonal mean temperatures in Finland during the last 160 years based on gridded temperature data. *International Journal of Climatology*, **30**, 2247–2256. DOI: `10.1002/joc.2046`.

Velashjerdi Farahani, A., J. Jokisalo, N. Korhonen, K. Jylhä, K. Ruosteenoja and R. Kosonen, 2021. Overheating Risk and Energy Demand of Nordic Old and New Apartment Buildings during Average and Extreme Weather Conditions under a Changing Climate. *Applied Sciences*, **11**. DOI: `10.3390/app11093972`.

Venäläinen, A., I. Lehtonen, M. Laapas, K. Ruosteenoja, O.-P. Tikkanen, H. Viiri, V.-P. Ikonen and H. Peltola, 2020. Climate change induces multiple risks to boreal forests and forestry in Finland: A literature review. *Global Change Biology*, **26**, 4178–4196. DOI: `10.1111/gcb.15183`.

Viljanen, K., X. Lü and J. Puttonen, 2020. "Hygrothermal Behaviour of Ventilation Cavities in Highly Insulated Envelopes". In: *E3S Web of Conferences, Volume 172*. Ed. by J. Kurnitski and T. Kalamees. 12th Nordic Symposium on Building Physics (NSB 2020), Tallinn, Estonia. DOI: `10.1051/e3sconf/202017200703`.

Weigel, A. P., R. Knutti, M. A. Liniger and C. Appenzeller, 2010. Risks of model weighting in multimodel climate projections. *J. Climate*, **23**, 4175–4191. DOI: `10.1175/2010JCLI3594.1`.

Supporting information

    This paper is accompanied by a supplement file that provides tabular information about the projected seasonal and annual mean changes of the mean temperature, precipitation, surface pressure, incident solar radiation, diurnal temperature range, and scalar wind speed (Tables S1–S6). Both the multi-model means and the 5 to 95 % probability intervals are given for three future periods and all four SSP scenarios. Changes simulated by the individual GCMs under SSP2-4.5 are listed in Tables S7 (for the period 2040–2069) and S8 (2070–2099). Monthly multi-model mean changes and uncertainty intervals for the six variables for the period 2070–2099 under SSP2-4.5 are presented in Fig. S2 (a similar representation as in Fig. 6). The geographical distributions of the multi-model mean changes of four climate quantities for the period 2070–2099 are shown in Figs. S3–S6 (to be compared with the spatial distributions for the period 2040–2069, presented in Figs. 10–13). Spatial distribution of the relative humidity change is shown in Fig. S7.